Native $SrTiO_3$ (001) surface layer from resonant Ti $L_{2,3}$ reflectance spectroscopy

S. M. Valvidares,[1,2] M. Huijben,[3,4] P. Yu,[3] R. Ramesh,[1,3] and J. B. Kortright[1]

[1]*Materials Sciences Division, Lawrence Berkeley National Laboratory, Berkeley, California 94720-8099 USA*

[2]*ALBA Synchrotron Light Source, 08290 Cerdanyola del Vallès, Barcelona, Spain*

[3]*Dept. of Physics, University of California, Berkeley, California 94720-809 USA*

[4]*Faculty of Science and Technology & MESA+ Institute for Nanotechnology, University of Twente, 7500 AE, Enschede, The Netherlands*

Abstract

We quantitatively model resonant Ti $L_{2,3}$ reflectivity $R_{s,p}(q, h\nu)$ from several $SrTiO_3$ (001) single crystals having different initial surface preparations and stored in ambient conditions before and between measurements. All samples exhibit unexpected 300 K $R_s(h\nu) - R_p(h\nu)$ anisotropy corresponding to weak linear dichroism and tetragonal distortion of the TiO_6 octahedra indicating a surface layer with properties different from cubic $SrTiO_3$. Oscillations in $R_s(q)$ confirm a ubiquitous surface layer 2-3 nm thick that evolves over a range of time scales. Resonant optical constant spectra derived from $R_{s,p}(h\nu)$ assuming a uniform sample are refined using a single surface layer to fit measured $R_s(q)$. Differences in surface layer and bulk optical properties indicate that the surface is significantly depleted in Sr and enriched in Ti and O. While consistent with the tendency of $SrTiO_3$ surfaces toward non-stoichiometry, this layer does not conform simply to existing models for the near surface region and apparently forms via room temperature surface reactions with the ambient. This new quantitative spectral modeling approach is generally applicable and has potential to study near-surface properties of a variety of systems with unique chemical and electronic sensitivities.

PACS: 68.47.Gh, 61.05.cm, 78.70.Dm, 78.20.Ci

I. INTRODUCTION

Oxides having the perovskite structure exhibit rich behavior of continued fundamental and applied interest. $SrTiO_3$ (STO) crystals are common substrates for epitaxial growth, and interest in STO continues to focus on near-surface properties of bulk crystals and, more recently, on emergent behavior with practical implications in heterostructures containing ultrathin STO films. The STO (001) surface exhibits complex structural behavior depending sensitively on thermochemical history [1]. Examples include different surface terminations [2], surface relaxation and reconstruction studied experimentally [3, 4, 5, 6, 7, 8, 9] and theoretically [10, 11, 12, 13, 14], and a strong propensity towards non-stoichiometry presumably resulting from high, differential diffusion and sublimation rates of cationic and anionic species that can result in decomposition reactions into Ruddelsden-Popper and Magneli phases and substantial subsurface composition variation with depth extending tens of nanometers below the surface [15, 16, 17]. Some of these surface-related phenomena manifest as lateral heterogeneity such as coexisting surface reconstructions or fast diffusion along line defects [16, 17], and most include in-depth heterogeneity to a greater or lesser degree. Considerable recent interest in ultrathin epitaxial $SrTiO_3$ films and their interfaces has been motivated by understanding dielectric breakdown in thin film capacitors [18], novel 2D electronic configurations localized at heterointerfaces [19, 20, 21], and the potential of strained films to bring ferroelectric functionality to Si-based and other devices [22, 23]. Presumably similar sensitivity to thermochemical history exists in such thin films and heterostructures, although additional gradients in chemical potential, strain, and polarization strongly influence chemical and physical properties and their stability [24]. To understand such systems there is a need for non-destructive techniques that can probe chemical

and physical properties with high sensitivity and depth resolution several to tens of nanometers *beneath* their top surface.

We were motivated to combine the high sensitivity of soft x-ray absorption spectroscopy (XAS) to local Ti electronic structure in such systems [25, 26, 27, 28, 29, 30] with angle-dependent specular reflectivity measurements known for penetrating, depth-resolving sensitivity. Analogous to modeling reflectance in the visible spectral range, the general goal of such a study is to quantitatively model specular reflectivity $R(q, h\nu)$ as a function of scattering vector q and photon energy $h\nu$ across a core resonance of interest to obtain a depth profile of the variation of resonant optical properties as described, *e.g.*, by the complex refractive index $n(h\nu) = 1 - \delta(h\nu) + i\,\beta(h\nu)$. While similar to many, related resonant soft x-ray scattering studies of magnetic [31, 32, 33, 34, 35, 36, 37, 38, 39], orbital [40, 41, 42, 43, 44], superlattice [45, 46, 47], and polymer [48, 49, 50, 51, 52] structure, the approach here is distinct in that it aims to determine resonant optical properties directly from reflectivity data rather than from ancillary XAS measurements, that are susceptible to measurement artifacts, or from theoretical models of resonant electronic structure. While several groups have modeled soft x-ray reflectivity to obtain resonant optical [53, 54] and magneto-optical [32, 33, 55] properties, it is not a common choice to obtain spectroscopic information nor commonly integrated with structural modeling as is done here.

This work began as part of a study of epitaxial of $SrTiO_3/SrRuO_3$ superlattices on $SrTiO_3$ (001) as a model system to understand dielectric breakdown in ultrathin STO layers [18] by studying their local Ti environments using resonant Ti $L_{2,3}$ reflectivity to probe into the superlattice structure. In this context, accurate resonant Ti optical spectra were sought from single crystals for comparison with spectra from the superlattice. Interest in the STO substrate

surface itself increased after we observed unexpected 300 K linear anisotropy, $R_s(h\nu) - R_p(h\nu)$, that was subsequently found to be localized in a ubiquitous surface layer ~ 2 – 3 nm thick with markedly different optical properties than the bulk. This surface layer does not conform neatly to existing models of STO surface properties, and instead results from room temperature surface reactions with atmospheric constituents following initial surface treatments and is observed to respond to changes in ambient conditions. We develop a quantitative approach to self-consistently model both the resonant $h\nu$ and q dependence of reflectivity data that is the basis for our understanding of this surface layer. Sections below detail modeling of $R(h\nu)$ to obtain accurate values of resonant optical constants, observation of linear anisotropy and dichroism in local Ti environments at room temperature near the STO surface, and modeling of $R(q, h\nu)$ to gain further insight into this surface layer. These modeling approaches, with some extension, are generally applicable to depth-resolve resonant optical properties in a range of systems. In the conclusions we comment briefly on the implications of these STO single crystal results for oxide crystals and heterostructures generally, especially as studied by techniques sensitive to surface or near-surface properties.

II. EXPERIMENTAL

Results from five $SrTiO_3$ (001) single crystals (samples A – E) are reported. Sample A was first and most studied, providing the bulk of results reported on. Samples B – E were studied to explore the generality of results first observed from A and possible effects of differences in initial surface preparation. All samples received a standard chemical-mechanical polish by the vendor (Crystec, GmbH). Sample A was then prepared as if for growth of epitaxial films using

standard approaches [56] in which a buffered HF etch removes the outer SrO monolayer to leave a TiO_2 terminated surface [2, 57], followed by a 3 hour anneal at 950 -1000 C in flowing O_2 to improve the terrace structure of the surface. Such surface treatment routinely yields RHEED patterns indicating highly ordered, smooth surfaces. Samples B – E received the following treatments, respectively: no treatment (as-received), HF etch only, HF etch followed by vacuum anneal (700C for 1 hr in 10^{-6} Torr), and HF etch followed by a similar O_2 anneal as for sample A. Such oxygen and vacuum annealing is reported to produce subsurface regions having substantially different average composition from stoichiometric $SrTiO_3$ [15, 16, 17], and vacuum annealing is well known to induce O vacancies enhancing conductivity and inducing a blue color. Following these treatments samples were stored in ambient atmospheric conditions prior to and between measurement sessions over the span of many months. Measurements were made in ultrahigh vacuum (10^{-8} – 10^{-9} Torr) at 300 K on numerous occasions, and on several occasions sample A was cooled to 20 K. Thus, while samples had prescribed initial treatments, their surfaces were free to evolve during long periods of atmospheric exposure and brief exposure to vacuum during measurement. We expect that the near-surface regions studied were in equilibrium with air at 300 K prior to measurements.

Specular reflectance $R_{s,p}(q, h\nu)$ was measured with vertical scattering plane at several beamlines (BL) at the Advanced Light Source including elliptically polarizing undulator BL 4.0.2 (*s* and *p* polarization), linearly polarized undulator BL 8.0 (*s* polarization), and bending magnet BL 6.3.2 (predominantly *s* polarization). $R(h\nu)$ was measured at fixed grazing incidence angle θ, with $h\nu$ varying across the Ti $L_{2,3}$ edges. $R(q)$ was measured at different, fixed $h\nu$ and for all data here $q = 4\pi\sin\theta/\lambda$ is oriented normal to the surface. Even at the highest q measured, the ratio of specular to off-specular diffuse intensity in the detector aperture was ≥ 10, so that

diffuse scattering from surface roughness or lateral heterogeneity does not contribute significantly to measured intensities. Samples were mounted with metal clips on their top surface, possibly mitigating charging effects and potential gradients that are reported to be severe in some electron spectroscopy studies [58]. Si diode detectors measured reflected intensities and the direct beam for normalization to absolute reflectance. In some cases total electron yield (TEY) XAS was measured via drain current simultaneously with $R(h\nu)$ measurements. Samples were exposed to synchrotron beams for extended and repeated periods and exhibited no changes in optical properties over time except for rather subtle effects reported below. While TEY measurements at 20 K showed occasional instabilities related to charging/discharging, we saw no indication of radiation induced changes in reflectivity measurements. Results reported here were reproducible between different measurement sessions and so are considered robust.

Modeling of $R(q, h\nu)$ data as discussed in several instances below was accomplished with an algorithm for global numerical minimization of an arbitrary error function metric allowing an arbitrary number of parameters to vary between adjustable constraints in defining the model $R(q, h\nu)$ [59]. The error function us used is defined as the average over all data points of the square of difference between model and data divided by the model or its square. Such weighting helps balance the contribution of all data points in the minimization. This flexible approach can be used fit a single data set or many data sets simultaneously with some or all parameters in common. We typically varied the limits between which spectral and structural parameters could vary in fitting to ensure that parameters defining best fits are insensitive to range constraints. The models we use below to fit data are all relatively simple and present no convergence problems unless otherwise noted. The quality of fits can thus be gauged visually.

III RESULTS AND DISCUSSION

III.1. Complex refractive index from reflectance spectra

Our initial goal with STO crystals was to determine accurate, absolute refractive index spectra across the Ti $L_{2,3}$ edges from measured reflectivity data $R(h\nu)$. Initially we had no reason to assume anything other than a semi-infinite slab described by a uniform, isotropic index

$$n_o = 1 - \delta_o + i\beta_o = 1 - \frac{r_e \lambda^2}{2\pi} \sum_j \rho_j (f_{1,j} + i f_{2,j}) \quad (1)$$

where $f_{1,j}(h\nu)$ and $f_{2,j}(h\nu)$ are the real and imaginary parts of the atomic scattering factor of elemental species i with number density ρ_i, and r_e is the electron radius [60]. We further assumed stoichiometric, cubic $SrTiO_3$ with lattice constant 0.391 nm. Optical constants δ_o and β_o (also f_1 and f_2) are related via a Kramers-Kronig (KK) dispersion relation constraining their independent variation. Model $R(h\nu)$ are obtained from the modulus squared of the complex s and p Fresnel reflectance amplitudes [61]. Because δ_o and β_o enter to the 2nd power and in cross-terms in reflected intensity expressions, reflectance spectra should be twice as sensitive to small changes in resonant features compared to direct XAS measurements. Reflectance amplitudes are generally reduced by a static Debye-Waller-like term, $e^{-\frac{1}{2}(\sigma q)^2}$, where σ represents the *rms* surface roughness and/or interdiffusion.

Fitting $R(h\nu)$ with this simplest structural model reduces to finding the shape of $n_o(h\nu)$ that best reproduces measured spectra. n_o is modeled with both non-resonant and resonant contributions as illustrated in Fig. 1, where measured (θ = 15°, 300 K) and best fit model $R_s(h\nu)$ are in the top panel. The sum of non-resonant Sr and O contributions plus the Ti 2-step (L_3 and

L_2) continuum absorption jump obtained from tabulated atomic scattering factors [62] and the expression above are blue lines in Figs. 1(b) and1(c). Regarding the resonant Ti contributions, the measured spectrum exhibits 4 dominant peaks, 2 each corresponding to transitions into empty t_{2g} and e_g states at the L_3 ($2p_{3/2}\rightarrow 3d$) and L_2 ($2p_{1/2}\rightarrow 3d$) edges. In addition 2 sharp, very weak peaks are below the L_3 t_{2g} peak, and 2 broad, weak features are observed near 473 and 478 eV. All of these peaks are well known from STO XAS studies [27, 28, 29, 30] in which Ti has a dominant formal Ti^{4+}, $d0$ configuration. The 6 peaks below 470 eV correspond to resonant dipole-allowed transitions into empty 3d states, while the 2 broader features above 470 eV have been discussed as excited state satellites of excitonic [27] or charge transfer [29] origin. We use Lorentzian line shapes (green lines in Figs. 1(b) and 1(c)) to describe the resonant contributions to β_o because their KK transforms yield analytical expressions for their dispersive contributions to δ_o so that only 3 parameters (position, width, intensity) per peak are varied to fit the experimental reflectivity as in Figure 1(a), avoiding the need for repeated KK evaluations [63, 64]. We chose to allow the resonant contributions to the 4 largest peaks to vary as fit parameters, to fix the contributions of the two weak peaks at 456.39 and 457.10 eV, and to ignore the high energy excited-state peaks for simplicity. As σ was not known initially, a factor was introduced to scale the model and data; its value was determined by matching at the extreme points of the data range where the resonant peaks make the smallest contributions.

This isotropic, semi-infinite slab model fits the intensity and shape of the 4 dominant reflectivity peaks well, yielding values for δ_o and β_o in Figs. 1(b)and 1(c) (red lines) that can be considered absolute within this model's accuracy. Figures 2(a) and 2(b) show the individual f_1 and f_2 spectra for Ti, O, and Sr obtained by decomposing δ_o and β_o according to (1). In subsequent sections we show that this homogeneous slab model does not adequately describe

these samples, and also that the results in Figs. 1(b) and 1(c) do give a reasonable first approximation of absolute Ti optical properties. This last point is important as it provides a general approach to modeling systems with unknown layered structure as demonstrated below.

Knowledge of absolute values of resonant optical properties is important for several reasons. Fundamentally, β determines the x-ray penetration depth $l_x(h\nu, \theta)$ indicating how far into a sample (normal to surface) we can sense material properties. For θ above the critical angle for total reflection, $l_x = \lambda \sin\theta / 4\pi\beta$. For STO l_x is a strong function of $h\nu$ across the Ti resonances as shown at θ = 15, 30, and 90° in Figure 3(b), decreasing by an order of magnitude at the t_{2g} and e_g lines from non-resonant values. Such short penetration depths (only 4 nm at the L_3 e_g line at θ = 15°) result from the strong and sharp absorption at the Ti $L_{2,3}$ lines that in turn result from the $d0$ configuration of Ti^{4+} in STO, yielding f_2 values ~200 electrons (Fig. 2(b)). The broadening and reduction of absorption features by multiplet splitting and increased filling of 3*d* states across this series implies that these STO values set an approximate lower limit for resonant l_x in 3*d* transition metal oxides. While such small resonant l_x values potentially limit studies of bulk properties, viewed from a different perspective they provide sensitivity to electronic structure in a subsurface region that is difficult for many characterization techniques to sense and, presumably, very relevant to functional interactions of materials with their environment.

Short skin depths exacerbate well-known saturation effects in common measures of XAS using partial or total electron yield (PEY or TEY) or fluorescence yield (FY), whereby the heights of the strongest absorption peaks relative to the continuum edge jump are suppressed when l_x becomes comparable to the escape depth l_e or l_f of the detected particles [25, 65, 66, 67]. This is demonstrated in Figure 3(a) where TEY- and reflectivity-derived $\beta_0(h\nu)$, both measured

at $\theta = 15°$, are compared. The 4 strongest absorption peaks are systematically weaker in TEY- compared to reflectivity-derived spectra, and this discrepancy increases with absorption. Models of saturation effects show that the intrinsic absorption spectrum is distorted by these relative probing lengths by $\frac{1}{1/l_x+1/l_e}$. Comparing relative L_3 line strengths and using l_x values determined here yields $l_e \cong 2.6$ nm. FY XAS spectra suffer from a similar saturation effect where the relevant escape depth l_f is that of the fluorescent x-ray [68]. The $h\nu$ dependence of l_f is that of l_x. Transitions filling photo-excited 2*p* core holes originate predominantly from the lowest lying 3*d* conduction band states, so the predominant fluorescence energy equals the excitation energy into the empty t_{2g} and e_g states in Fig. 1(a). l_f is thus significantly reduced by resonant absorption, although measuring fluorescence emitted normal to the surface yields $l_f > l_x$ for off-normal incidence. Saturation effects are thus more significant in FY than in TEY detection. The strong energy dependence of l_x may be particularly important in resonant x-ray emission spectroscopy, where sensing depth depends on both incident and emitted x-ray energies in a way that could yield very different sensing depths for different features.

Accurate absolute XAS cross sections may provide new insights when modeling spectra with theoretical electronic structure calculations. Comparisons of theoretical and experimental spectra typically rely on relative spectral shapes and intensities, with little regard for absolute values. Artifact-free spectra should provide impetus to compare absolute intensities between theory and experiment, and may reveal subtle spectral features of strong absorption peaks not apparent otherwise. While detailed comparison with theoretical spectra is beyond the scope of this paper, we did evaluate atomic multiplet spectra for *d*0 Ti^{4+} in O_h and converted intensities from dipole line strength to f_2 oscillator strength values [69], finding that experimental values of ~ 200 electrons at the L_3 peaks are consistent with such models.

Reflectivity-derived optical constant spectra are expected to be relatively free of measurement artifacts and so to provide reliable absolute β values of material within several l_x of the surface. Artifacts that could influence reflectivity-derived β spectra include harmonic content in the incident beam spectrum and contributions of inelastic scattering (including fluorescence and resonant inelastic scattering) to measured intensities. Inelastic contributions are generally weak compared to specular intensities, and significant harmonic content is easily observed and eliminated in the incident beam and further reduced on specular reflection that acts as a low-pass filter. An implicit assumption here is that structural aspects of the sample are known and included in the modeling process. Samples described by the semi-infinite slab model are simple to model, while samples heterogeneous in depth complicate the modeling process to obtain reliable optical constants as considered below.

III.2. Room-temperature anisotropy in near-surface region

To explore the sensitivity of $R(h\nu)$ to subtle changes in electronic structure we reasoned that cubic STO at 300 K should be isotropic, while below the antiferrodistortive (AFD) transition at T_{AFD} = 110 K some anisotropy ($R_s(h\nu) - R_p(h\nu) \neq 0$) should be observed corresponding to a linear dichroism (LD) associated with the tetragonal character in the AFD phase. Thus we measured R_s and R_p from sample A at 300 and 88 K, modeled spectra as above, and evaluated $R_s - R_p$. Contrary to expectation, weak anisotropy was observed at 300 K. R_s and R_p were measured at $\theta = 15°$, and R_p was corrected by the polarization factor for Thompson scattering ($\cos^2 2\theta$) to compare with R_s in Figs. 4(a) and 4(b). Anisotropy spectra are in Figs. 4(c) and 4(d), and in all panels symbols represent measured data and lines are model fits. The Lorentzian

resonant β_o model fits the features of $R_s - R_p$ quite well. Figure 5 shows the model β_o spectra (top panels) and corresponding LD (bottom panels) resulting from the fits in Figure 4.

The relatively small (~10 %) size of the unexpected 300 K reflectance anisotropy prompted much repeated measurement to convince ourselves that it is real. The anisotropy in the Ti environment is clearly resonant in nature, vanishing off resonance. Of the 2 sets of t_{2g} and e_g peaks, the L_3 t_{2g} peak is the sharpest and is resolution limited. This became clear when we observed that $R_s - R_p$ sometimes displayed a derivative line shape, only at this line, whose bipolar shape changed sign in comparing different data sets indicating subtle incident beam energy drifts between or during collection of individual datasets. The L_3 t_{2g} anisotropy in Fig. 4 does not suffer from this artifact, leading us to believe that these results best represent the sample response. The large e_g anisotropy compared to the weak t_{2g} anisotropy cannot be explained by artifacts that would produce energy-independent intensity shifts between *s* and *p* polarization. Its observed T dependence suggests the anisotropy itself is real. Most importantly, repeated measurements on this sample and 300 K measurements on samples D-E (not shown) all indicate similar, reproducible anisotropy shapes (aside from occasional L_3 t_{2g} derivative line shape as noted).

Assuming resonant electric dipole (E1) transitions dominate, this Ti $L_{2,3}$ anisotropy must result from a subtle, non-cubic distortion in the average Ti environment determined primarily by the TiO_6 octahedra. While this distortion could easily be static in nature, it is possible that anisotropic vibrations of Ti within the octahedra could also yield weak dichroism [70], although if this were the case a larger T dependence than observed might be expected. Compared to LD observed in Ti_2O_3 [71], that observed here is weak, which is not surprising given the very different average Ti environments and formal charge state. We are unaware of LD

measurements of TiO_2 in its different forms. The 300 K LD is predominantly in the e_g peaks that probe antibonding d_z^2 and $d_{x^2-y^2}$ states pointing towards and hybridizing strongly with the O 2*p* states [28]. The t_{2g} peaks probe antibonding d_{xy}-like states that point towards the octahedra face centers and hybridize more weakly with the O 2*p* states. Given these relative hybridization differences of Ti e_g and t_{2g} states with O 2*p* states we expect stronger LD in e_g peaks than in t_{2g} peaks, as the stronger hybridization channel should be more sensitive to any non-cubic distortion of tetragonal symmetry. The small but clearly observable 0.025 eV shift of the leading edge of the antibonding L_3 e_g peak to higher energy for *s* relative to *p* polarization indicates that the in-plane $d_{x^2-y^2}$ orbital is more strongly hybridized with O 2*p* states than is the out-of-plane d_z^2 orbital, as would result from a tetragonal distortion of the TiO_6 octahedra elongated normal to the surface.

Similar weak LD has been recently observed in TEY XAS from a $SrTiO_3$ (001) crystal [72] and from a tetragonally distorted, 5 unit cell thick STO epitaxial film on Si (001) under compressive strain [73]. In these studies theoretical spectral models indicate a tetragonal distortion stretched along the surface normal. We calculated ligand field multiplet spectra of Ti^{4+} in O_h and D_{4h} that confirm theoretical results of these other studies, all of which are consistent with the symmetry considerations above. We stress that the LD observed here and in these other studies can be interpreted in terms of non-cubic Ti point symmetry that might involve a ferroelectric (FE) or antiferroelectric (AFE) distortions, but that we cannot resolve non-centrosymmetric character from this measurement alone.

At 88 K the Ti $L_{2,3}$ LD has changed and the t_{2g} lines as well as the e_g lines exhibit significant anisotropy suggesting a further reduction in symmetry. Even though a non-cubic distortion exists at 300 K, it is natural to consider whether a distortion similar to that in the low T AFD

phase of $SrTiO_3$ in which the TiO_6 octahedra rotate in a staggered fashion about the tetragonal axis [74, 75, 76], accounts for the anisotropy changes in going from 300 to 88 K. Distortions away from centered cubic or centered tetragonal symmetry are expected to change hybridization between the t_{2g} states and O 2*p* states more significantly than does the distortion from centered cubic to centered tetragonal. Thus the reduction of symmetry below centered tetragonal as in the AFD phase can be expected to induce LD in the t_{2g} lines along with the e_g lines, as observed in the 88 K data. Again this is suggestive of FE or AFE distortions, but is not conclusive evidence.

The 300 K data are clearly inconsistent with cubic symmetry however, and taken together these linear anisotropy results indicate that the surface or some part of the near surface region exhibits reduced symmetry above T_{AFD}. This is distinctly at odds with isotropic, cubic STO and thus indicates that a more complicated near-surface structure exists.

Several possible origins of this 300 K LD suggest themselves. First, the truncated surface of an otherwise cubic crystal must exhibit some LD simply because of the surface termination. Second, structural relaxation (including possible FE distortion) within the first 2-3 unit cells of an STO (001) surface has been observed using hard x-ray crystal truncation rod and electron diffraction techniques [3, 4, 5, 6, 7, 8, 9] and in first principles theoretical studies [10, 11, 12, 13, 14]. These studies generally find relaxation of atomic positions predominantly outward and sometimes inward along the surface normal and rumpling (separation of metal and oxygen ion positions along the normal) in the first monolayer, although fine details may differ between different studies. Third, knowing that $SrTiO_3$ is prone to non-stoichiometry and that its (001) surface responds to both reducing and oxidizing environments [1, 15, 16, 17], especially at elevated T, some chemically modified, non-stoichiometric subsurface layer(s) can be anticipated in this sample (A) since it was O_2-annealed. Finally, exposure to air for prolonged periods

almost certainly leaves residual H_2O or OH^- monolayer at the surface [77, 78, 79], and given the high diffusivities of O and Sr (and H) and the tendency of STO toward non-stoichiometry, it is not unexpected that surface reactions could result in a metastable surface layer in near equilibrium between the atmosphere and a nominal ideal bulk STO crystal. All of these possibilities could contribute to the observed weak anisotropy, could easily be operative at some level, and are necessarily associated with the surface or near-surface region. The short skin depths at the Ti lines and strong resonant sensitivity to local electronic structure suggest that resonant q-resolved reflectivity should be well-suited to study possible depth variations in near-surface optical properties.

III.3. Ubiquitous surface layer from $R(q)$

We explored these possibilities by measuring $R_s(q)$ at several energies across the Ti $L_{2,3}$ edge, finding that all samples exhibit an interference oscillation confirming the presence of a surface layer distinct from the bulk and, furthermore, that this layer evolves with time. Modeling the q and $h\nu$ dependence of these data provides semi-quantitative understanding of the nature of this layer. Below we first discuss general trends and then review some systematics of modeling $R(q)$ from sample A measured at different times and energies.

Normalized $R(q)/R_F(q)$ at 440 eV for all five samples are plotted in Figure 6, where R_F is the Fresnel reflectivity for a semi-infinite slab calculated using sample A optical constants derived as above (taking σ = 0.15 nm). At this energy l_x is large as β_o is small, although an appreciable resonant δ_o persists (Figs. 1 & 2). While details differ between samples, they all exhibit a pronounced oscillation, also known as a Kiessig or thickness fringe [80], signaling the presence of a surface layer having substantially different optical properties and presumably composition

than the bulk of the samples. Modeling these data as described below indicates that the thicknesses of these layers range from roughly 1.5 – 2.7 nm.

The surface layer in sample A was observed to evolve with time. Temporal evolution was initially deduced from changes in position of the interference minimum in different measurement sessions widely separated in time, and was subsequently explored by repeated measurements during a given session. Figure 7(a) shows 3 of 4 such $R(q)$ profiles measured at 440 eV and relative times t (in the same session) as noted, together with R_F. Figure 7(b) shows corresponding R/R_F and fits obtained by simultaneously modeling all 4 datasets with a single layer model (details below) having the same surface layer optical properties n_{surf} allowing independent variation only of layer thickness d for each dataset. d is generally determined by the oscillation period, not its phase or minima positions that depend sensitively on δ, although for fixed n these features also vary with d as in Fig. 7. It was not possible to fit these data with common d by varying only n_{surf} for each layer. Resulting d values display linear t dependence in Figure 8 that is uninterrupted during a 2 hour period when the x-ray beam was off, so that this temporal evolution is not radiation induced. While d increased by roughly 0.5 nm in this 5 hour period, measurements on the same sample in prior measurement sessions yield best fit d values ranging from 1.9 – 3.2 nm with no monotonic temporal trend. The layer's thickness thus oscillates over longer time scales than monitored in Fig. 8. The $R_s(q)$ modeled and discussed below were collected in the same session as these data to minimize questions about changes in the surface layer between measurement sessions. The trends in Fig. 8 suggest that the surface is evolving in response to the disturbance of a metastable equilibrium with air when it is introduced into vacuum.

The existence of the surface layer obviously implies that $n_o(h\nu)$ derived above using the semi-infinite slab model is at best an approximate description of the optical properties $n_{sub}(h\nu)$ and $n_{surf}(h\nu)$ of the substrate and surface layer, respectively. While structurally refining the semi-infinite slab model with single- and multilayer models is straight-forward [61], it is less obvious how to refine resonant n_{sub} and n_{surf} in fitting $R_s(q, h\nu)$. Indeed it was not initially obvious that the surface layer is derived from $SrTiO_3$ or composed of something else entirely. Our approach here is to systematically alter $n_o(h\nu)$ derived as above to refine n_{sub} and n_{surf} in a manner that preserves KK consistency by allowing the linear superposition of Sr, Ti, and O contributions vary according to eqn. (1), noting again that the Ti contribution is separable into resonant and non-resonant parts. For the substrate (assumed isotropic) we start with $n_{sub} = (n_{o,s}+n_{o,p})/2$ and vary only the strength of the resonant Ti part by a scaling factor (1 parameter) in fitting. These n_o spectra were obtained assuming stoichiometric $SrTiO_3$ non-resonant contributions, which similarly applies to the non-resonant part of n_{sub}. n_{surf} is refined from $n_{o,s}$ with all elemental non-resonant and resonant (intensity only) contributions free for refinement (4 parameters). While elemental contributions are varied in fitting, it is the resulting δ_{surf} and β_{surf} that determine the fit, which thus does not necessarily result from a unique layer constitution because the optical properties for Sr and O (Fig. 2) are roughly energy independent and so can compensate for each other in fitting. We observed this behavior when fits of equal quality resulted from slight variations of parameter range limits yielding rather different apparent layer compositions but nearly equal n_{surf} values. Thus we present best fit n_{surf} values below rather than effective surface layer compositions, and find subsequently that their trends with $h\nu$ do inform us on the make-up of the surface layer relative to the bulk.

Using this prescription for refinement of n_{surf} and n_{sub} we fitted individual R/R_F datasets at 8 energies. These data and best fit results are in Figure 9. The single frequency Keissig fringe in R/R_F is evident at higher q, while most datasets show more complex structure at lower q resulting at least in part from normalization of the layered sample R by R_{Fres} representing a semi-infinite sample. Considerable $h\nu$-dependent phase shifts in the thickness fringe result from expected large resonant refractive effects. Single layer models generally reproduce all of these features; somewhat better at non-resonant (Figs. 9(a), (b), (h)) compared to resonant (Figs. 9(c) – (g)) energies, with only the lowest q region at 459.84 eV not reproduced. The slightly poorer fits at the resonant energies suggest a slight gradient in surface layer Ti content, since at these energies Ti dominates optical properties while at non-resonant energies the scattering factors of all elements are of the same order of magnitude (Fig. 2). Not surprisingly, a 2-layer model significantly improves the low q fit at 495.84 eV (Fig. 9(f)). The resulting top surface and interface σ values from the single layer fits are less than 0.35 nm indicating smooth interfaces.

Comparing best fit n_{surf} and n_{sub} at these discrete energies with the $n_o(h\nu)$ spectrum in Fig. 10(a) reveals that the model optical constant values are very close to and follow all resonant trends of $n_o(h\nu)$. This indicates that n_o is a good starting point for refining the surface layer and bulk optical properties in a 1-layer model, and also that the deviations away from n_o by the n_{surf} and n_{sub} fit results should provide meaningful information about how these two materials differ from each other. Significantly, the strong resonant character of the n_{surf} spectrum indicates that Ti is present in the surface layer and, thus, that it derives from the STO substrate.

Trends in best fit β_{surf} and β_{sub} values with $h\nu$ in Fig. 10(a) indicate how the surface layer and bulk differ. Away from the resonant absorption lines $\beta_{surf} < \beta_{sub}$, and according to eqn. (1) and

Fig. 2 this implies significant depletion in Sr that dominates β in these regions. When tuned to the lines $\beta_{surf} > \beta_{sub}$ indicating stronger resonant absorption in the surface layer that in turn implies enrichment in Ti in the surface layer because the intrinsic absorption strength of the Ti^{4+}, $d0$ configuration cannot increase. These trends are substantiated by simultaneously modeling the best fit n_{surf} and n_{sub} values (both δ and β) in Fig. 10(a) with optical constants parameterized as in fitting $R(q)$ in Fig. 9 to obtain surface layer and bulk constitutions that best describe these collected fit values. The resulting fits are superposed with the same discrete n_{surf} and n_{sub} values in Fig. 10(b), where the nominal constitutions yielding these fit spectra are also given. The resulting substrate values (blue lines) change from n_0 by a 30% reduction in the resonant Ti contribution, and represent our best estimate of the resonant optical properties for stoichiometric, cubic STO. The best fit surface layer values (red lines), while not matching the discrete n_{surf} values as well as for the substrate, depart substantially from n_0 in agreement with the observations above. The model has the surface layer depleted in Sr volume density to 1/3 that of n_0 to account for the decreased non-resonant absorption, and enhanced in resonant Ti density by 1/3 compared to n_0. This model also predicts an enhancement in O density by 2/3, which together with the Ti enhancement is suggestive of a surface layer enriched in TiO_2.

While this $R(q, h\nu)$ spectroscopic modeling approach of refining an initial estimate of $n_o(h\nu)$ to a more realistic pair of $n_{surf}(h\nu)$ and $n_{sub}(h\nu)$ spectra in a layered structural model represents an advance in methodology, several cautionary indicators defer claims of absolute surface layer composition determination. One is the ill-conditioned nature of fitting with respect to variations of flat Sr and O contributions. Another is that the surface layer is evolving in time so the notion of a distinct composition can itself be questioned. Another is that the layer evidently contains a weak gradient. Yet another is that, given the initial oxidizing annealing treatment of this sample,

the assumption that the region below the surface layer is stoichoimetric STO is questionable. Finally, the model for resonant Ti contributions of the substrate and surface layer (intensity only variation of absorption lines of fixed shape & position) is likely to be oversimplified. We see opportunities for more flexible variation of resonant optical spectra, and additional self-consistency iterations that should result in more robust fitting algorithms. Measuring $R(q)$ at many more energies across the Ti edge should aid in implementing more flexible spectral models, and modeling spectra across the O edge, for example, would also bring new information to improve modeling. Nonetheless, trends in these modeling results provide meaningful understanding of the nature of the near surface region. For example, the evident surface depletion in Sr is at odds with composition depth profiles of similarly O_2 annealed samples that report a surface significantly enriched in Sr and a deeper layer enriched in Ti resulting from differential diffusion of Sr and Ti, with the faster diffusing Sr species reaching the surface first [16]. This is further evidence that the surface layer observed here forms after the initial O_2 annealing treatment, presumably at RT in response to atmospheric exposure.

Comparison of these $R(q)$ results with hard x-ray surface diffraction results [4, 6, 7, 8, 9] is instructive for several reasons since both approaches measure x-ray intensities vs. vertical momentum transfer q. The reciprocal space domains of soft x-ray $R(q)$ and hard x-ray crystal truncation and surface superlattice rods (CTR & SSR, respectively) are very different in ways that bear directly on their structural sensitivity. Near the Ti L_{23} edge we are limited by λ to roughly the $q < 4$ nm^{-1} range and to measuring only the specular reflectivity, that is equivalent to the specular (00) CTR when the miss-cut angle is zero. These hard x-ray studies typically measure perpendicular momentum transfers over a range of roughly 4 – 56 nm^{-1} that does not overlap significantly with the low q range sampled here. Furthermore, to study both lateral and

vertical deviations in atomic positions in surface reconstructions the surface diffraction techniques ignore the specular rod, and instead measure vertical momentum transfer along low index CTRs and SSRs (xy) with integer or fractional x and y. Their high q range for both in-plane and perpendicular directions acts as a high-pass filter emphasizing information from the most ordered part of the surface region to yield sub-angstrom precision in modeling surface relaxation. However, structural information from more disordered atomic arrangements in a surface layer, should they exist, can be attenuated in the high-q range precisely because of their disorder [81]. Conversely, the low q soft x-ray range precludes interatomic sensitivity [82], and instead senses a significantly blurred scattering contrast defined in terms of n that spatially averages atomic scattering factors. The intrinsic sensitivity of the soft and hard x-ray measurements is thus quite different, with each emphasizing different structural aspects.

The reconstructions determined in these surface diffraction studies, and related theoretical studies [5, 10, 11, 12, 5, 13], are not consistent with the $R(q)$ measured here. Surface relaxations obtained from these studies are generally characterized by near-surface rearrangements extending no more than 2 or 3 unit cells (~1 nm) into the crystal, rather small (less than several %) deviations from bulk density averaged over this depth, and changes in effective stoichiometry, if they exist, only in the outermost monolayer. Such reconstruction models cannot describe the $R(q)$ modeled here, whose observed structure requires larger optical contrast and layer thickness than predicted by these CTR models. While a TiO_2 double layer at the surface has been reported [5, 8], consistent with the composition trend in the surface layer observed here, this double layer is not consistent with the soft x-ray results that require a much thicker region of TiO_2 enrichment. The differences in the surface layers observed here and the surface reconstructions observed in diffraction experiments can be understood to result either

from real differences in near surface structure owing to different sample histories, from differences in structural sensitivity in the presence of disorder, or both.

IV. CONCLUSIONS

We observe a ubiquitous surface layer that is distinct from surface reconstructions deduced from surface diffraction studies or first principles theory, and also distinct from subsurface composition variations of freshly annealed samples resulting from differential diffusion as determined by SIMS. Unexpected linear anisotropy in $R(h\nu)$ and the Keissig fringe in $R(q)$ are clear evidence for this layer, that derives from $SrTiO_3$ but has a distinctly different composition from the underlying substrate. We cannot completely rule out the possibility that the layer is a vestige of chemical-mechanical polishing by the vendor, but its temporal evolution on both long and short time scales indicates that it responds to changes in ambient conditions so that it does result at least partly and could result entirely from reactions with the ambient. The layer's response to changes in ambient pressure even at 300 K indicate that it could form quickly and does form via diffusion in response to chemical driving forces between ambient and condensed phase constituents. The layer's finite thickness suggests that the surface reaction is diffusion-limited. The surface layer is thus in some ways analogous to a passivating native oxide layer on Si or Al, with a significant difference being that on STO this layer is not passive and rather responds readily to changes in ambient chemical potential even at room temperature. While the existence of such a layer is not surprising, given the known propensity of STO surfaces toward non-stoichiometry, we are unaware of non-destructive techniques that have observed and quantified this layer and its evolution with time. This can be understood by realizing that

resonant soft x-ray reflectivity is not commonly used in as extensive a manner as we have done here, taking advantage simultaneously its spectroscopic sensitivity to symmetry via polarization, composition differences through modeling, and direct depth-resolving capabilities.

Several aspects of the spectroscopy are noteworthy. Considering the short penetration depths when tuned to the strong absorption lines, we conclude that the weak LD observed also at these lines originates in the surface layer. While we cannot rule out anisotropic vibrations or ferroelectric distortions as the source for this weak anisotropy, the apparent surface depletion in Sr and enrichment in Ti and O suggests that the composition change is correlated with distortions in the average Ti environments yielding the LD. We emphasize, however, that the t_{2g} and e_g lines derived from the semi-infinite slab model and refined by the surface layer model are not consistent with additional multiplet splitting that results from significant distortions of the TiO_6 octahedra as in TiO_2 [27, 28, 29] or from the presence of Ti^{3+} as in Ti_2O_3 [71]. While we do not claim to have refined the optical constant spectra well enough to resolve subtle differences in spectral shape, there is little indication that resonant Ti lines are significantly broadened or shifted in the overlayer compared to the bulk. This is difficult to reconcile with a significantly modified surface composition that would presumably tend toward more distortion in structure and hence spectra as in TiO_2. If the bulk crystal structure templates the surface layer as in epitaxy, this would help explain the apparent weak departure from cubic symmetry in the surface layer having substantially different composition. We suggest that H^+ diffusion into the surface layer to replace Sr^+ may also help to maintain relatively cubic structure, and hypothesize that this may be occurring.

We became aware of the surface layer only by observing unexpected linear anisotropy in $R(h\nu)$ and Kiessig fringes in $R(q)$, and this has several implications considering the continued

fundamental and technological interest in oxide surfaces and interfaces. Because we did not set out to study a surface layer on STO, these results leave many unanswered questions as noted. Studies designed to follow surface layer formation and its response to different thermochemical conditions would clearly be interesting both for STO and for other oxide surfaces to explore the generality of such a surface layer. Other implications relate to resonant soft x-ray spectroscopic characterization, and indeed any characterization of oxide crystals, heteroepitaxial films, and nanoparticles that is primarily sensitive to near-surface properties. Such layers evidently may be present without our knowledge, especially on samples exposed to ambient conditions, in which case results from such techniques could lead to spurious interpretations. Presumably surfaces freshly cleaved or prepared in UHV chambers would be less susceptible to such surface layer formation.

The approach developed here, that combines measured resonant reflectivity spectra (including their anisotropy) and *q*-resolved reflectivity with quantitative, self-consistent modeling to obtain optical constants for the surface layer and bulk regions directly from the reflectivity data, represents an advance in methodology that demonstrates the power of resonant reflectivity as a spectroscopic tool that compares favorably with more commonly used spectroscopies in the soft x-ray range. The approach provides direct information on the depth variation of electronic and chemical properties from the depth variation of optical constants. Reflectivity is relatively free of measurement artifacts such as saturation effects and thus yields accurate, absolute resonant spectroscopic quantities. The analysis of the relatively simple $SrTiO_3$ surfaces studied here yielded unanticipated findings that resulted from combining relatively simple structural and spectroscopic models. In general, modeling the depth variation of resonant optical properties is expected to require more flexible algorithms allowing for more variation of

resonant spectral features and their anisotropy with depth, and possibly more densely measured data to resolve finer spectroscopic detail. As such approaches are developed the utility of this resonant x-ray reflectivity spectroscopy approach should grow.

Acknowledgements

Research, including measurements using beamlines 4.0, 8.0, and 6.3.2 at the Advanced Light Source (LBNL), was supported by the U. S. Dept. of Energy, Office of Basic Energy Sciences, Division of Materials Sciences and Engineering under Contract No. DE-AC02-05CH11231. A U. S. – Spain Fulbright supported SMV for part of this work.

References

1. D. A. Bonnell and J. Garra, Rep. Prog. Phys. **71**, 044501 (2008) and references therein.
2. M. Kawasaki, K. Takahashi, T. Maeda, R. Tsuchiya, M. Shinohara, O. Ishiyama, T. Yonezawa, M. Yoshimoto, and H. Koinuma, Science **266**, 1540 (1994).
3. N. Bickel, G. Schmidt, K. Heinz, and K. Muller, Phys. Rev. Lett. **62**, 2009 (1989).
4. G. Charlton, S. Brennan, C. A. Muryn, R. McGrath, D. Norman, T. S. Turner, and G. Thornton, Surf. Sci. **457**, L376 (2000).
5. N. Erdman, K. R. Poeppelmeier, M. Asta, O. Warschkow, D. E. Ellis, and L. D. Marks, Nature **419**, 55 (2002).
6. V. Vonk, S. Konings, G. J. van Hummel, S. Harkema, and H. Graafsma, Surf. Sci. **595**, 183 (2005).
7. R. Herger, P. R. Willmott, O. Bunk, C. M. Schleputz, B. D. Patterson, and B. Delley, Phys. Rev. Lett. **98**, 076102 (2007).
8. R. Herger, P. R. Willmott, O. Bunk, C. M. Schleputz, B. D. Patterson, B. Delley, V. L. Shneerson, P. F. Lyman, and D. K. Saldin, Phys. Rev. B **76**, 195435 (2007).
9. A. Fragneto, G. M. De Luca, R. Di Capua, U. S. di Uccio, M. Salluzzo, X. Torrelles, T. L. Lee, and J. Zegenhagen, Appl. Phys. Lett. **91**, 3 (2007).
10. V. Ravikumar, D. Wolf, and V. P. Dravid, Phys. Rev. Lett. **74**, 960 (1995).
11. J. Padilla, and D. Vanderbilt, Phys. Rev. B **56**, 1625 (1997).

12. J. Padilla, and D. Vanderbilt, Surf. Sci. **418**, 64 (1998).
13. R. I. Eglitis, and D. Vanderbilt, Phys. Rev. B **77**, 195408 (2008).
14. J. L. Wang, M. Fu, X. S. Wu, and D. M. Bai, J. Appl. Phys. **105**, 083526 (2009).
15. K. Szot, M. Pawelczyk, J. Herion, C. Freiburg, J. Albers, R. Waser, J. Hulliger, J. Kwapulinski, and J. Dec, Appl. Phys. A-Mater. Sci. Process. **62**, 335 (1996).
16. K. Szot, W. Speier, J. Herion, and C. Freiburg, Appl. Phys. A-Mater. Sci. Process. **64**, 55 (1997).
17. K. Szot and W. Speier, Phys. Rev. B **60**, 5909 (1999).
18. M. Stengel, and N. A. Spaldin, Nature **443**, 679 (2006) and references therin.
19. A. Ohtomo, D. A. Muller, J. L. Grazul, and H. Y. Hwang, Nature **419**, 378 (2002).
20. A. Ohtomo, and H. Y. Hwang, Nature **427**, 423 (2004).
21. A. Brinkman, M. Huijben, M. Van Zalk, J. Huijben, U. Zeitler, J. C. Maan, W. G. Van der Wiel, G. Rijnders, D. H. A. Blank, and H. Hilgenkamp, Nature Mater. **6**, 493 (2007).
22. J. H. Haeni, P. Irvin, W. Chang, R. Uecker, P. Reiche, Y. L. Li, S. Choudhury, W. Tian, M. E. Hawley, B. Craigo, A. K. Tagantsev, X. Q. Pan, S. K. Streiffer, L. Q. Chen, S. W. Kirchoefer, J. Levy, and D. G. Schlom, Nature **430**, 758 (2004).
23. M. P. Warusawithana, C. Cen, C. R. Sleasman, J. C. Woicik, Y. L. Li, L. F. Kourkoutis, J. A. Klug, H. Li, P. Ryan, L. P. Wang, M. Bedzyk, D. A. Muller, L. Q. Chen, J. Levy, and D. G. Schlom, Science **324**, 367 (2009).
24. N. Nakagawa, H. Y. Hwang, and D. A. Muller, Nature Mater. **5**, 204 (2006).
25. J. Stohr, *NEXAFS Spectroscopy* (Springer-Verlag, Berlin, 1992).
26. F. deGroot and A. Kotani, *Core Level Spectroscopy of Solids* (CRC Press, Boca Raton, 2008).
27. G. vanderLaan, Phys. Rev. B **41**, 12366 (1990).
28. F. M. F. deGroot, J. C. Fuggle, B. T. Thole, and G. A. Sawatzky, Phys. Rev. B **41**, 928 (1990).
29. K. Okada and A. Kotani, J. Electron Spectrosc. Related Phenom. **62**, 131 (1993).
30. F. M. F. Degroot, J. Electron Spectrosc. Related Phenom. **67**, 529 (1994).
31. C. C. Kao, C. T. Chen, E. D. Johnson, J. B. Hastings, H. J. Lin, G. H. Ho, G. Meigs, J. M. Brot, S. L. Hulbert, Y. U. Idzerda, and C. Vettier, Phys. Rev. B **50**, 9599 (1994).

32. J. M. Tonnerre, L. Seve, D. Raoux, G. Soullie, B. Rodmacq, and P. Wolfers, Phys. Rev. Lett. **75**, 740 (1995).
33. M. Sacchi, C. F. Hague, L. Pasquali, A. Mirone, J. M. Mariot, P. Isberg, E. M. Gullikson, and J. H. Underwood, Phys. Rev. Lett. **81**, 1521 (1998).
34. H. A. Durr, E. Dudzik, S. S. Dhesi, J. B. Goedkoop, G. van der Laan, M. Belakhovsky, C. Mocuta, A. Marty, and Y. Samson, Science **284**, 2166 (1999).
35. J. B. Kortright, S. K. Kim, G. P. Denbeaux, G. Zeltzer, K. Takano, and E. E. Fullerton, Phys. Rev. B **64**, 092401 (2001).
36. O. Hellwig, D. T. Margulies, B. Lengsfield, E. E. Fullerton, and J. B. Kortright, Appl. Phys. Lett. **80**, 1234 (2002).
37. S. B. Wilkins, P. D. Hatton, M. D. Roper, D. Prabhakaran, and A. T. Boothroyd, Phys. Rev. Lett. **90**, 187201 (2003).
38. E. Weschke, H. Ott, E. Schierle, C. Schussler-Langeheine, D. V. Vyalikh, G. Kaindl, V. Leiner, M. Ay, T. Schmitte, H. Zabel, and P. J. Jensen, Phys. Rev. Lett. **93**, 157204 (2004).
39. S. Roy, M. R. Fitzsimmons, S. Park, M. Dorn, O. Petracic, I. V. Roshchin, Z. P. Li, X. Batlle, R. Morales, A. Misra, X. Zhang, K. Chesnel, J. B. Kortright, S. K. Sinha, and I. K. Schuller, Phys. Rev. Lett. **95**, 047201 (2005).
40. P. Abbamonte, L. Venema, A. Rusydi, G. A. Sawatzky, G. Logvenov, and I. Bozovic, Science **297**, 581 (2002).
41. K. J. Thomas, J. P. Hill, S. Grenier, Y. J. Kim, P. Abbamonte, L. Venema, A. Rusydi, Y. Tomioka, Y. Tokura, D. F. McMorrow, G. Sawatzky, and M. van Veenendaal, Phys. Rev. Lett. **92**, 237204 (2004).
42. S. S. Dhesi, A. Mirone, C. De Nadai, P. Ohresser, P. Bencok, N. B. Brookes, P. Reutler, A. Revcolevschi, A. Tagliaferri, O. Toulemonde, and G. van der Laan, Phys. Rev. Lett. **92**, 056403 (2004).
43. P. Abbamonte, A. Rusydi, S. Smadici, G. D. Gu, G. A. Sawatzky, and D. L. Feng, Nature Physics **1**, 155 (2005).
44. D. J. Huang, H. J. Lin, J. Okamoto, K. S. Chao, H. T. Jeng, G. Y. Guo, C. H. Hsu, C. M. Huang, D. C. Ling, W. B. Wu, C. S. Yang, and C. T. Chen, Phys. Rev. Lett. **96**, 096401 (2006).

45. J. Chakhalian, J. W. Freeland, G. Srajer, J. Strempfer, G. Khaliullin, J. C. Cezar, T. Charlton, R. Dalgliesh, C. Bernhard, G. Cristiani, H. U. Habermeier, and B. Keimer, Nature Physics **2**, 244 (2006).
46. S. Smadici, P. Abbamonte, A. Bhattacharya, X. F. Zhai, B. Jiang, A. Rusydi, J. N. Eckstein, S. D. Bader, and J. M. Zuo, Phys. Rev. Lett. **99**, 196404 (2007).
47. H. Wadati, D. G. Hawthorn, J. Geck, T. Higuchi, Y. Hikita, H. Y. Hwang, L. F. Kourkoutis, D. A. Muller, S. W. Huang, D. J. Huang, H. J. Lin, C. Schussler-Langeheine, H. H. Wu, E. Schierle, E. Weschke, N. J. C. Ingle, and G. A. Sawatzky, J. Appl. Phys. **106**, 083705 (2009).
48. G. E. Mitchell, B. G. Landes, J. Lyons, B. J. Kern, M. J. Devon, I. Koprinarov, E. M. Gullikson, and J. B. Kortright, Appl. Phys. Lett. **89**, 044101 (2006).
49. T. Araki, H. Ade, J. M. Stubbs, D. C. Sundberg, G. E. Mitchell, J. B. Kortright, and A. L. D. Kilcoyne,, Appl. Phys. Lett. **89**, 124106 (2006).
50. C. Wang, T. Araki, and H. Ade, Appl. Phys. Lett. **87**, 214109 (2005).
51. J. M. Virgili, Y. F. Tao, J. B. Kortright, N. P. Balsara, and R. A. Segalman, Macromolecules **40**, 2092 (2007).
52. G. E. Stein, J. A. Liddle, A. L. Aquila, and E. M. Gullikson, Macromolecules **43**, 433 (2010).
53. I. Diel, J. Friedrich, C. Kunz, S. DiFonzo, B. R. Muller, and W. Jark, Applied Optics **36**, 6376 (1997).
54. R. Soufli, A. L. Aquila, F. Salmassi, M. Fernandez-Perea, and E. M. Gullikson, Applied Optics **47**, 4633 (2008).
55. J. E. Prieto, F. Heigl, O. Krupin, G. Kaindl, and K. Starke, Phys. Rev. B **68**, 134453 (2003).
56. G. Koster, B. L. Kropman, G. Rijnders, D. H. A. Blank, and H. Rogalla, Appl. Phys. Lett. **73**, 2920 (1998).
57. Reference 8 presents evidence that a single etch be insufficient to remove all cationic contaminants present on as-received surfaces.
58. J. Szade, B. Psiuk, M. Pilch, R. Waser, and K. Szot, Appl. Phys. A-Mater. Sci. Process. **97**, 449 (2009).
59. We utilized the NMinimize routine in Wolfram Mathematica 7, Wolfram Research, Inc.

60. R. W. James, *The Optical Principles of the Diffraction of X-Rays* (Ox Bow Press, Woodbridge, Connecticut, 1982).
61. L. G. Parratt, Phys. Rev. **95**, 359 (1954).
62. B. L. Henke, E. M. Gullikson, and J. C. Davis, At. Data Nucl. Data Tables **54**, 181 (1993).
63. C. D. Keefe, J. Mol. Spectrosc. **205**, 261 (2001).
64. A single Lorentzian for each absorption peak does not rigorously satisfy the odd symmetry requirement for KK transformation that is satisfied by adding a 2^{nd}, symmetry-odd Lorentzian (see Ref. 63). We neglect this 2^{nd} peak with negligible error considering the small ratio of peak width to position in the x-ray range.
65. S. V. Pepper, J. Opt. Soc. Am. **60**, 805 (1970).
66. G. Vanderlaan, and B. T. Thole, J. Electron Spectrosc. Related Phenom. **46**, 123 (1988).
67. Y. U. Idzerda, C. T. Chen, H. J. Lin, G. Meigs, G. H. Ho, and C. C. Kao, Nucl. Instr. & Meth. A **347**, 134 (1994).
68. F. M. F. Degroot, M. A. Arrio, P. Sainctavit, C. Cartier, and C. T. Chen, Solid State Commun. **92**, 991 (1994).
69. R. D. Cowan, *The Theory of Atomic Structure and Spectra* (University of California Press, Berkeley, 1981).
70. S. Tinte and E. L. Shirley, J. Phys.-Condes. Matter **20**, 6 (2008).
71. H. Sato, A. Tanaka, M. Sawada, F. Iga, K. Tsuji, M. Tsubota, M. Takemura, K. Yaji, M. Nagira, A. Kimura, T. Takabatake, H. Namatame, and M. Taniguchi, J. Phys. Soc. Jap. **75**, 053702 (2006).
72. M. Salluzzo, J. C. Cezar, N. B. Brookes, V. Bisogni, G. M. DeLuca, C. Richter, S. Thiel, J. Mannhart, M. Huijben, A. Brinkman, G. Rijnders, and G. Ghiringhelli, Phys. Rev. Lett. **102** , 166804 (2009).
73. J. C. Woicik, E. L. Shirley, C. S. Hellberg, K. E. Anderson, S. Sambasivan, D. A. Fischer, B. D. Chapman, E. A. Stern, P. Ryan, D. L. Ederer, and H. Li, Phys. Rev. B **75**, 140103 (2007).
74. P. A. Fleury, J. F. Scott, and J. M. Worlock, Phys. Rev. Lett. **21**, 16 (1968).
75. J. F. Scott, Rev. Mod. Phys. **46**, 83 (1974).
76. W. Zhong, and D. Vanderbilt, Phys. Rev. Lett. **74**, 2587 (1995).
77. V. E. Henrich, G. Dresselhaus, and H. J. Zeiger, Solid State Commun. **24**, 623 (1977).

78. S. Ferrer, and G. A. Somorjai, Surf. Sci. **94**, 41 (1980).
79. J. M. Pan, B. L. Maschhoff, U. Diebold, and T. E. Madey, J. Vac. Sci. Technol. A-Vac. Surf. Films **10**, 2470 (1992).
80. H. Kiessig, Annalen Der Physik **10**, 769 (1931).
81. J. B. Kortright and A. Bienenstock, Phys. Rev. B **37**, 2979 (1988).
82. While we cannot resolve interatomic distances with these soft x-ray measurements, we can clearly observe dimensional changes with deep sub-wavelength precision (λ = 2.8 nm) as shown in Figs. 7 & 8.

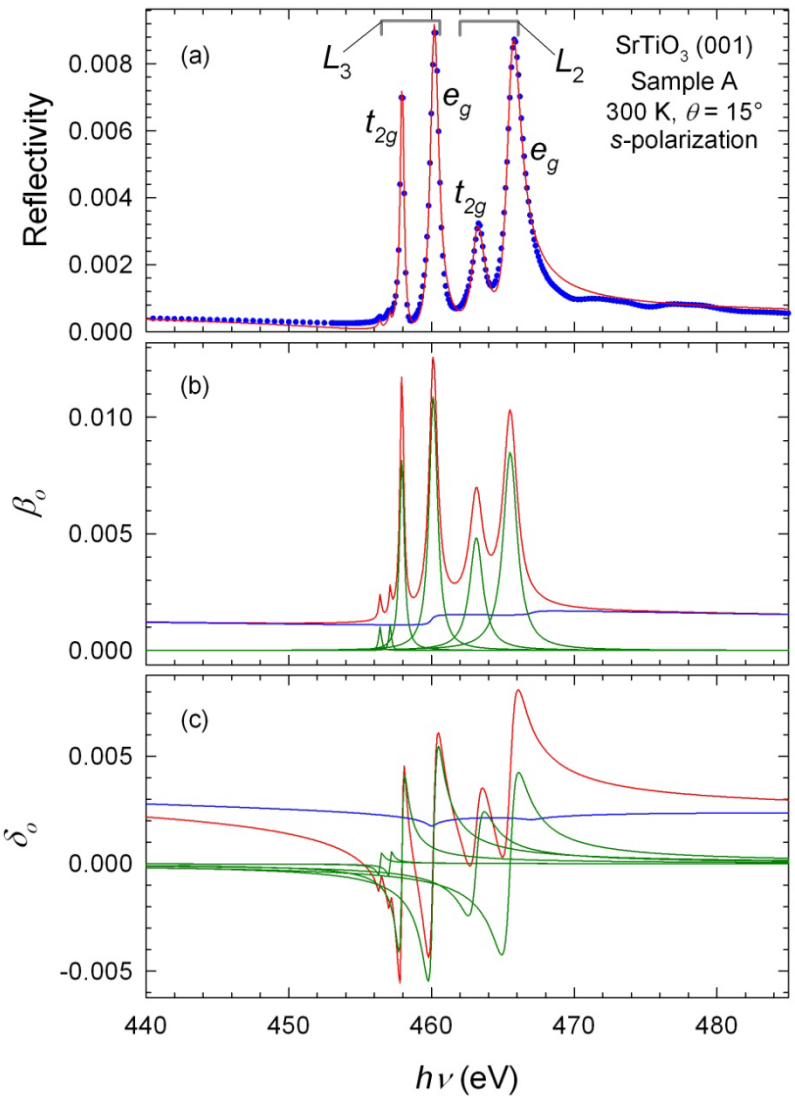

Figure 1. (Color online) (a) Measured reflectivity spectra (symbols) from $SrTiO_3$ (001) sample A together with model fit (line). (b) and (c) show, respectively, the best fit model β and δ (red) that are superpositions of non-resonant (blue) contributions of Sr, O, and the Ti 2-step continuum and six resonant peaks (green) described by Lorentzians. Fitting allowed the position, width and intensity of the 4 strongest Lorentzians to vary.

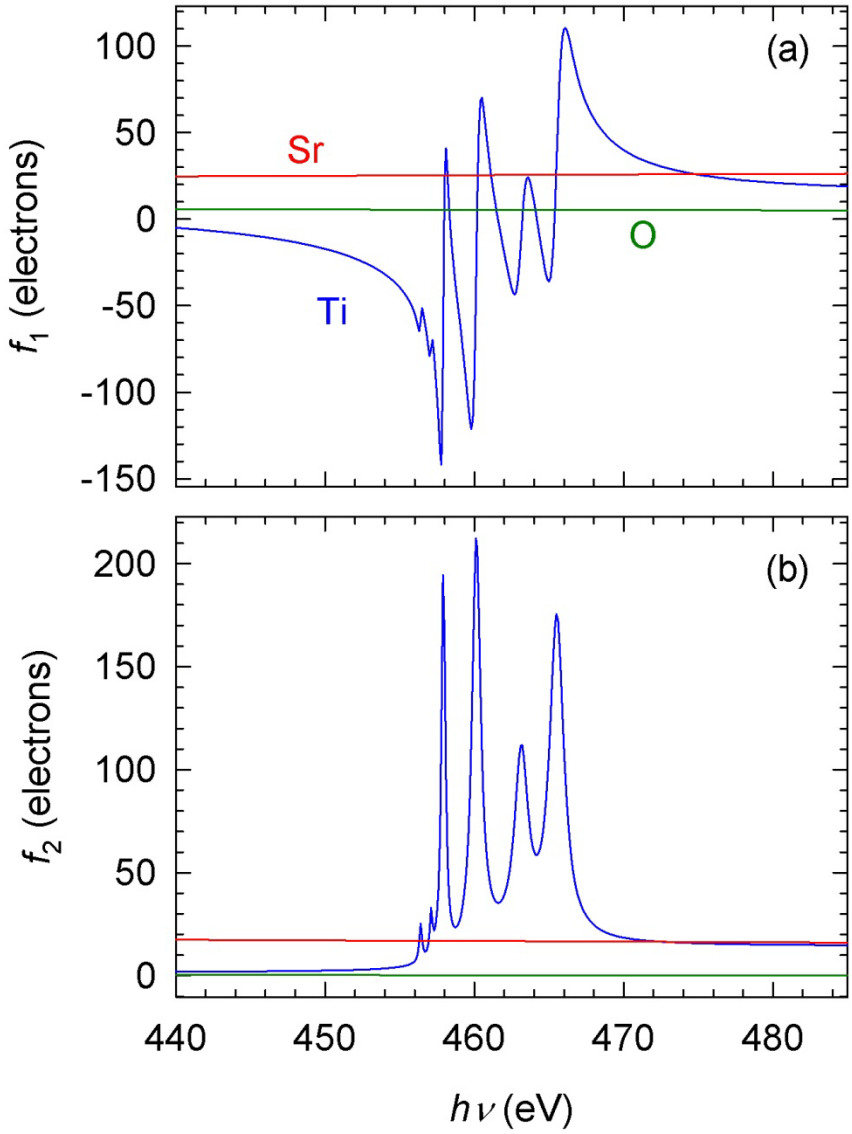

Figure 2. (Color online) (a) and (b) show atomic scattering factors f_1 and f_2 for Ti, O, and Sr across the Ti $L_{2,3}$ edges derived from best fit δ_o and β_o. Resonant and non-resonant (continuum) Ti contributions are summed. See text for details.

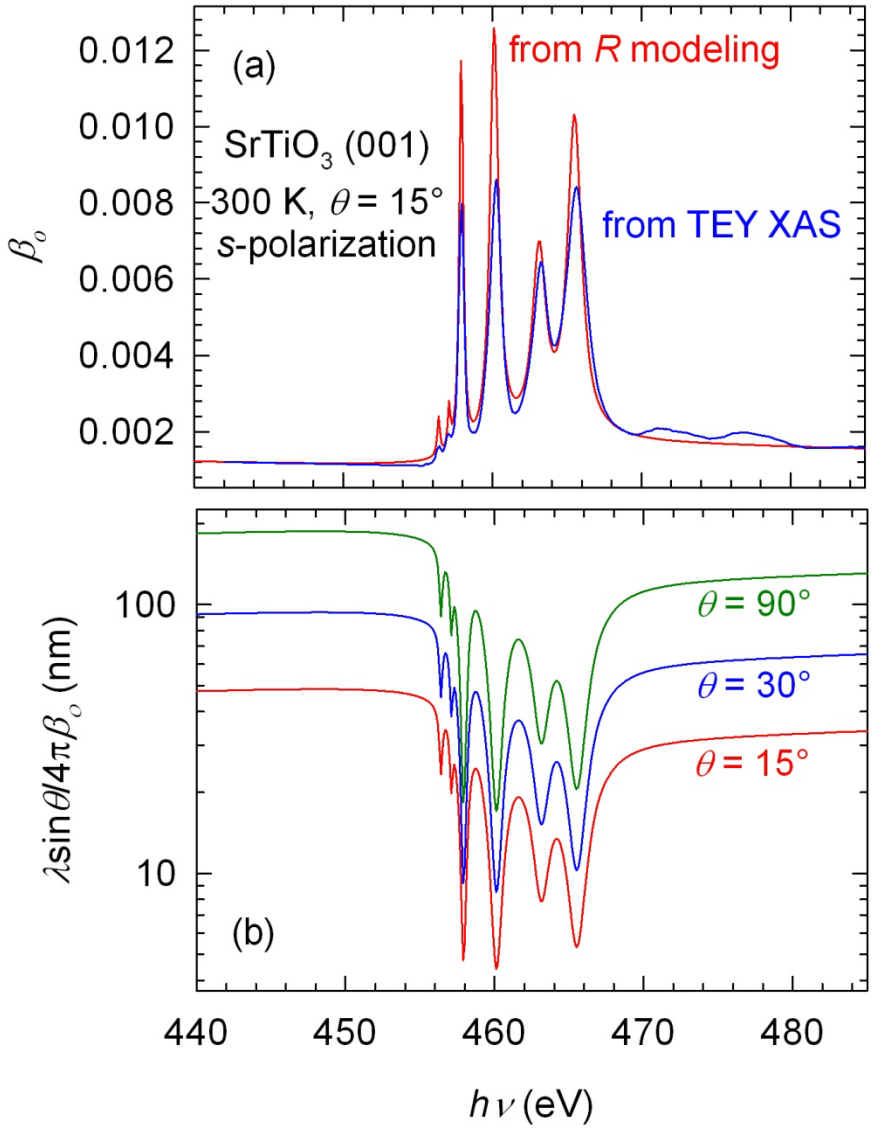

Figure 3. (Color online) (a) Comparison of β_o obtained from modeling $SrTiO_3$ (001) reflectivity and TEY absorption spectra (for sample A). (b) X-ray penetration depth determined from reflectivity-derived β_o.

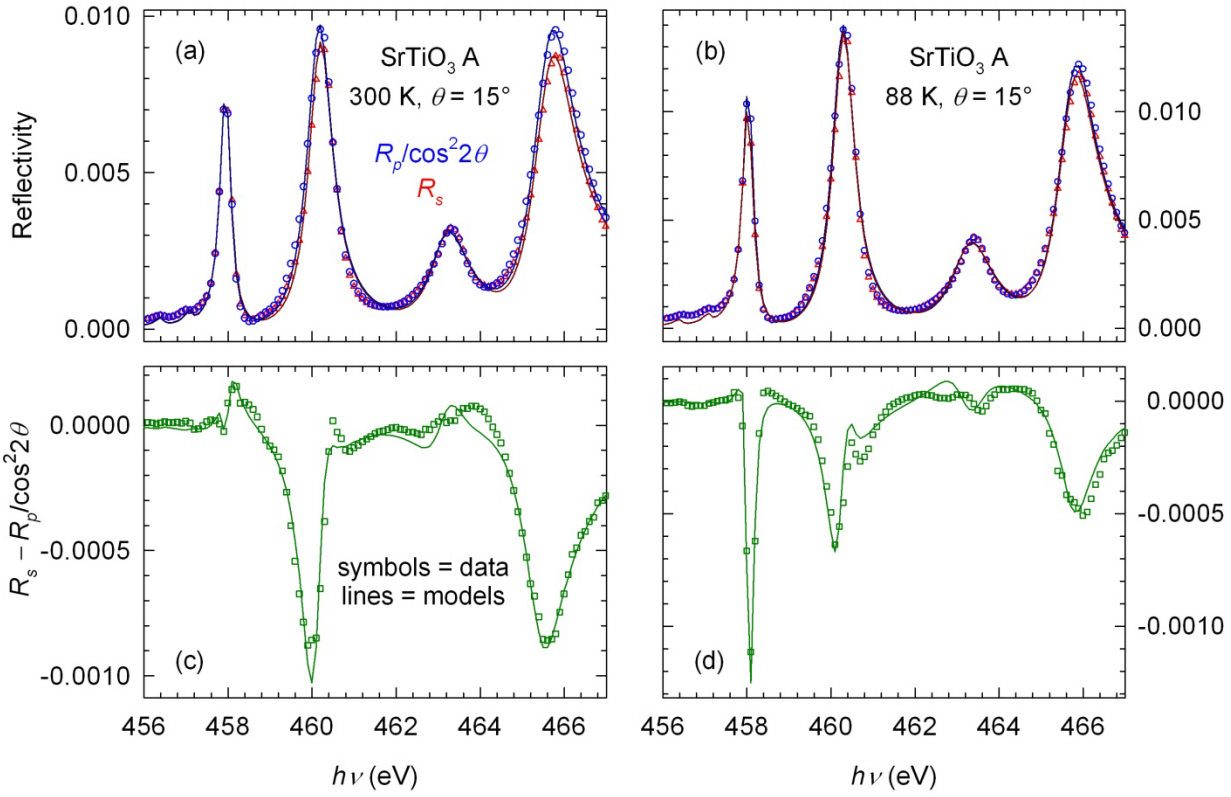

Figure 4. (Color online) Reflection spectra across the Ti $L_{2,3}$ edge from $SrTiO_3$ (001) sample A measured at $\theta = 15°$ using *s*- and *p*-polarization. (a) and (b) show $R_{s,p}(h\nu)$ measured at 300 and 88 K, respectively. (c) and (d) show reflection anisotropy $R_s - R_p$ at these temperatures. Measured data are symbols, best-fit models are lines.

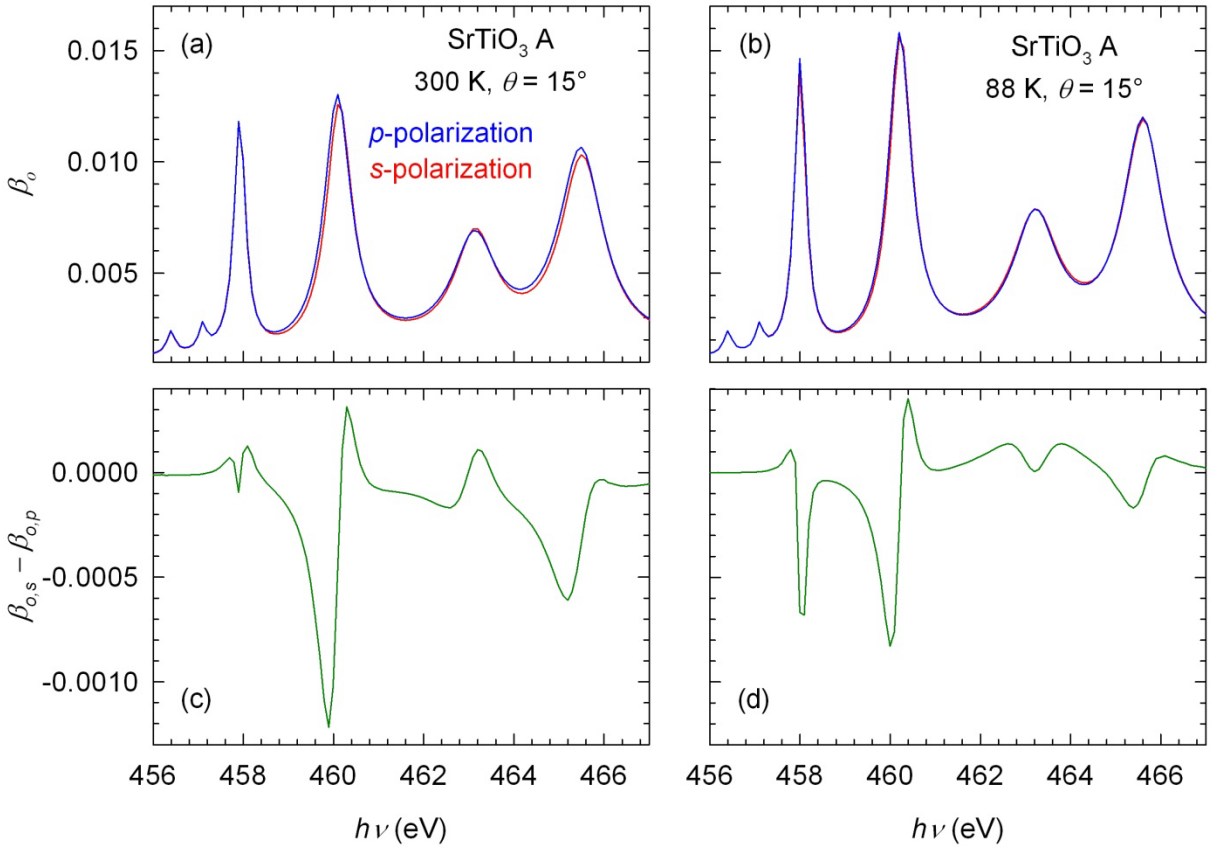

Figure 5. (Color online) Absorption index $\beta_o(h\nu)$ obtained from fitting $R_{s,p}(h\nu)$ at 300 and 88 K are in (a) and (b), respectively. Linear dichroism $\beta_{o,s} - \beta_{o,p}$ are in (c) and (d).

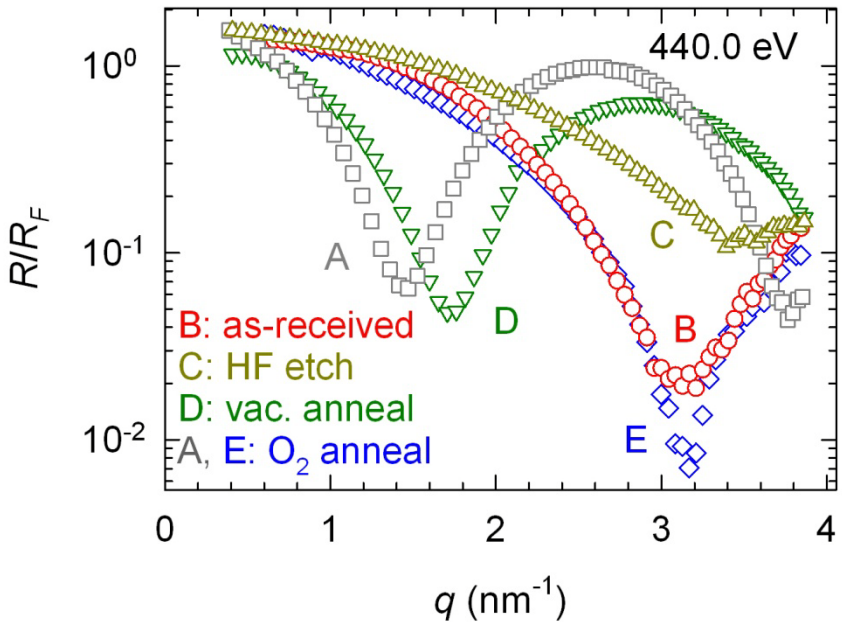

Figure 6. (Color online) Specular reflectivity for samples A-E measured at 440 eV and normalized by calculated Fresnel reflectivity R_F. A ubiquitous oscillation indicates the presence of an optically distinct surface layer.

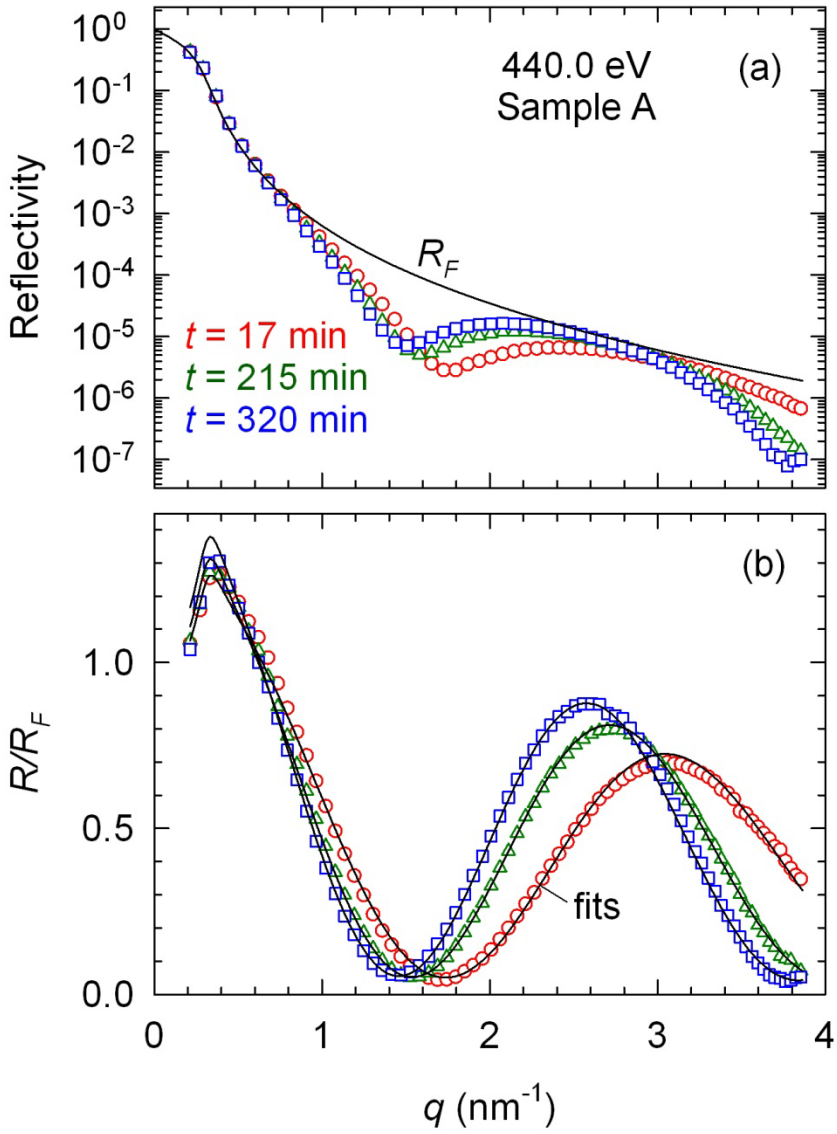

Figure 7. (Color online) Reflectivity scans at 440 eV from sample A measured at different relative times as noted. (a) shows $R(q)$ on a log scale together with R_F calculated using measured optical constants. (b) shows $R(q)/ R_F$ together with fits as described in the text.

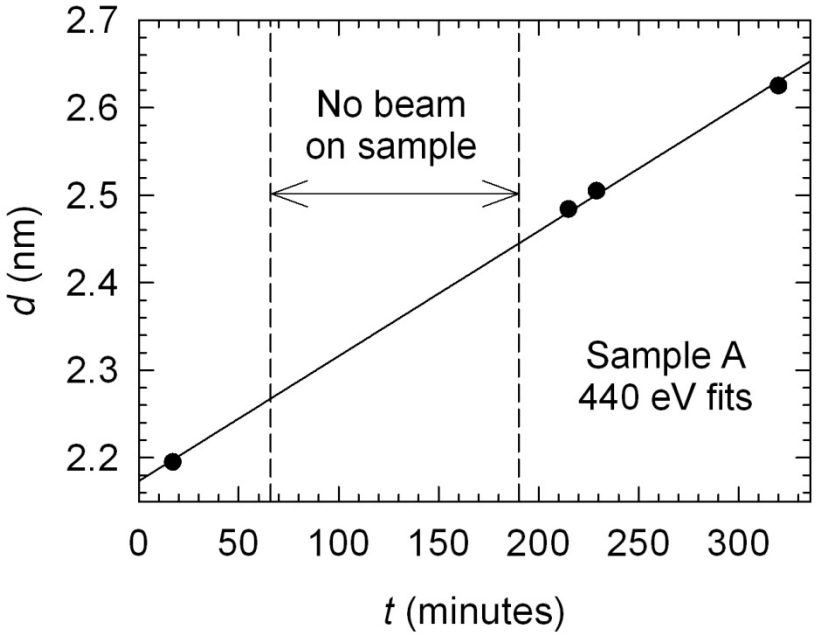

Figure 8. Evolution of sample A surface layer thickness with time obtained from modeling $R(q)$ as in Figure 7. The linear time dependence is uninterrupted during a period when the x-ray beam was off, confirming that the temporal evolution is not radiation-induced.

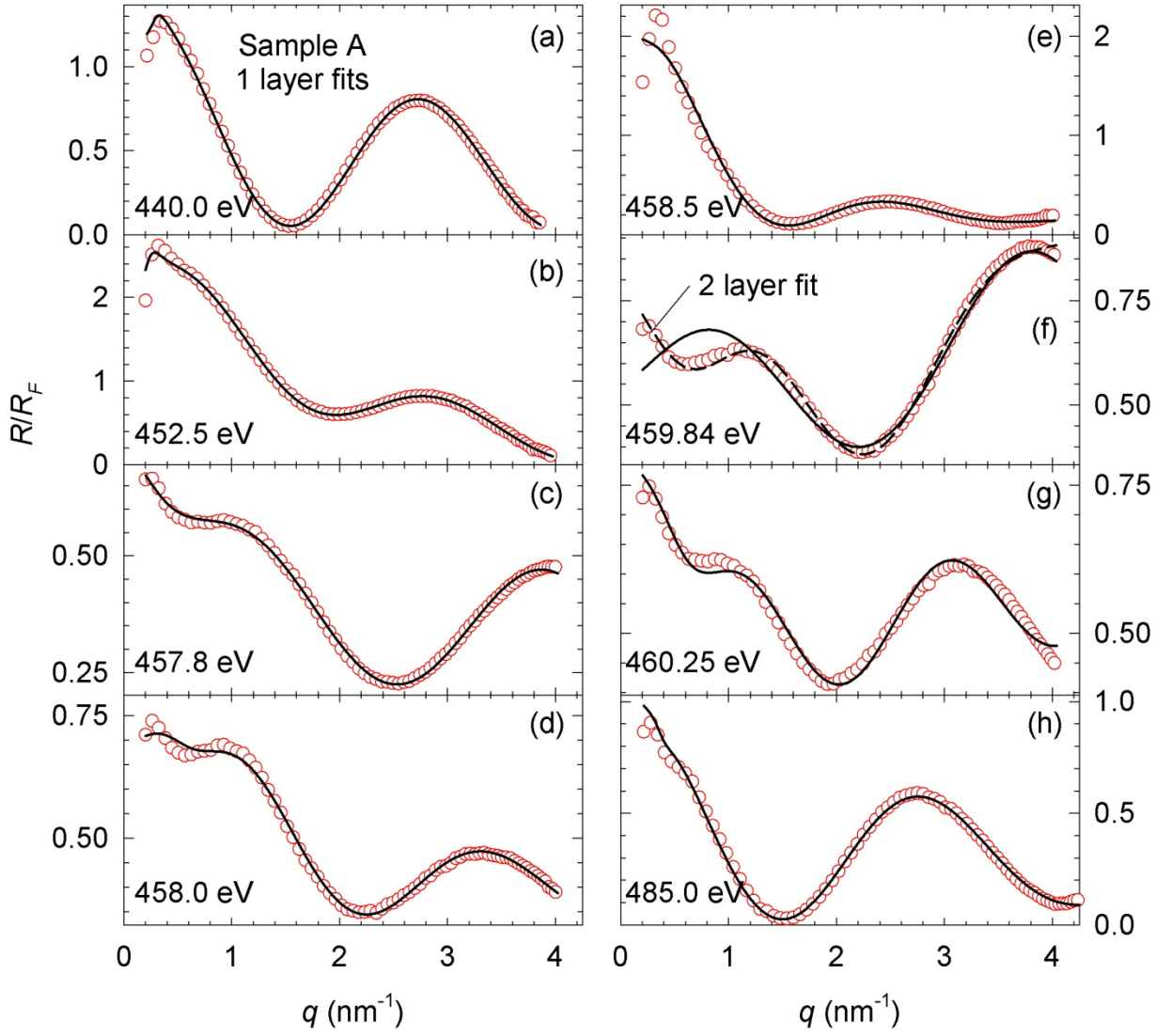

Figure 9. (Color online) Normalized sample A specular reflectivity R/R_F at energies noted. Measured data are symbols and solid lines are fits using a single surface layer model as described in the text. In (f) a 2-layer fit (dashed line) is also shown.

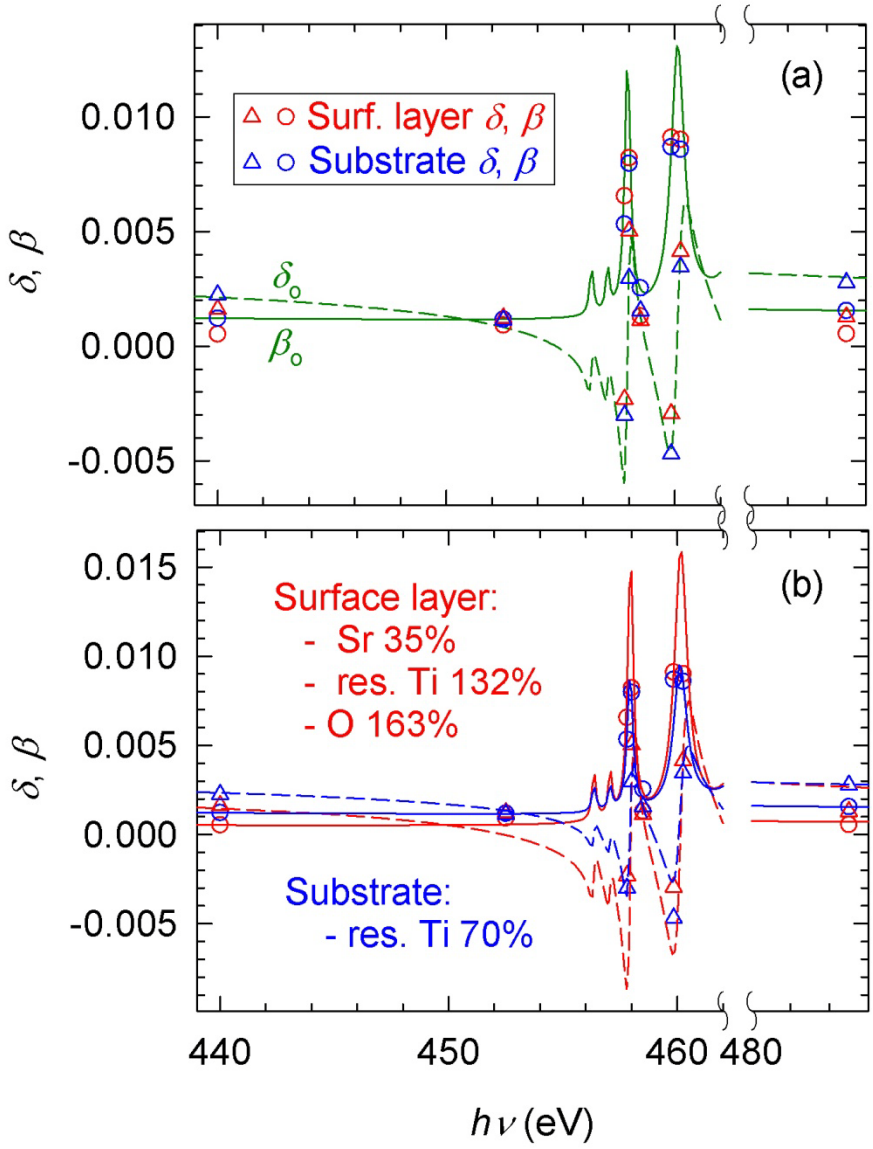

Figure 10. (Color online) Optical constants δ (triangles) & β (circles) from the single layer fits in Figure 9 are superimposed in (a) with the polarization averaged values (lines) assumed as the starting point to describe the isotropic substrate, and in (b) with the results of fitting the spectral dependence of these fit results at 8 discrete energies as described in the text.

LEGAL DISCLAIMER